Available online at www.sciencedirect.com

SciVerse ScienceDirect

Ceramics International 39 (2013) 403–413

CERAMICS INTERNATIONAL

www.elsevier.com/locate/ceramint

Effect of various pore formers on the microstructural development of tape-cast porous ceramics

Ayhan Sarikaya, Fatih Dogan*

Department of Materials Science and Engineering, Missouri University of Science and Technology, Rolla, MO 65409-0340, USA

Received 20 March 2012; received in revised form 6 June 2012; accepted 14 June 2012
Available online 21 June 2012

Abstract

Various types of pore formers have been used for the fabrication of ceramics with controlled porosity. This study addresses a detailed and systematic comparison of different pore formers (e.g. graphite, polymethyl methacrylate, sucrose and polystyrene) with distinct features such as size, distribution and morphology of particles and decomposition/oxidation behavior. Investigations also involve their effect on the rheological properties of the slurries and the microstructural development of laminated porous ceramic tapes.

Morphological features of the pore former particles were characterized using laser diffraction, B.E.T. surface area measurement and scanning electron microscopy (SEM) techniques as their thermal decomposition/oxidation behavior were determined by thermogravimetric analysis (TGA) and differential thermal analysis (DTA) methods. Tape compositions were developed and optimized in order to incorporate identical volumetric loadings of the materials in the tape formulations with different pore formers for a reliable comparison of their pore forming characteristics. Porous yttria stabilized zirconia (YSZ) ceramics were fabricated without macroscopic defects (e.g. cracks, warpage and delamination) by developing heating profiles based on the identified thermal properties of the pore formers. Characterization of the sintered porous ceramics by SEM and mercury intrusion porosimetry techniques revealed novel relationships between the physical properties of the utilized pore formers, processing parameters and final pore structures.

Keywords: A. Tape casting; B. Porosity; E. Fuel cells; Pore former

1. Introduction

Porous ceramics are essential for a wide range of engineering applications including separation membranes [1], filters [2], piezoelectric [3] and pyroelectric ceramics [4], lightweight structural materials [5], biomaterials [6], battery separators [7] and solid oxide fuel cell (SOFC) electrodes [8–10]. Controlling the features of the porosity in ceramic microstructures is crucial to satisfy the requirements of desired applications. For instance, uniform distribution of pores gives rise to the electrochemical performance of SOFC electrodes while their connectivity/percolation allows transport of the reactant and product gases efficiently [11–13].

Although there are numerous techniques to fabricate porous ceramics such as combustion synthesis [14,15], foaming [16], reactive infiltration [17], freeze drying [18] pyrolysis of polymeric precursors [19], electrophoretic deposition [20] and gel-casting [21], partial sintering of ceramic tapes [22,23] and incorporation of pyrolyzable pore formers to tape casting slurries [8,24,25] are commonly employed methods to fabricate tape-cast porous ceramics. In partial sintering, densification is retarded in order to obtain a certain amount of porosity. However, partial sintering has fundamental difficulties in controlling the essential features of porosity such as shape, size, distribution and connectivity of the pores. Moreover, a desired dense ceramic matrix cannot be formed since the ceramic particles are allowed only to form neck and create a skeleton. Thus, porous ceramics fabricated by partial sintering are poor in mechanical strength [8,26].

Pore former additions to the ceramic mixtures yield stable pores after the removal of the binder and the pore former particles. Formed pores are not removed at subsequent

*Corresponding author. Tel.: +1 573 341 7130; fax: +1 573 341 6934.
E-mail address: doganf@mst.edu (F. Dogan).

0272-8842/$36.00
http://dx.doi.org/10.1016/j.ceramint.2012.06.041

sintering steps [26,27] and the final porosity of the ceramic microstructures resemble the features of the pore former particles even after sintering at elevated temperatures [26,28,29]. Considering that amount, size, shape and thermal properties of the pore formers can be controlled, this technique has more control over the features of the porosity as well as mechanical properties of the ceramic matrix. By controlling the properties of the pore formers, the ceramic microstructures can be also tailored by means of sintering shrinkage which is critical for the fabrication of multilayer tape-cast ceramics. Controlled sintering shrinkage and combination of tape casting with lamination also allow the fabrication of multilayer structures which involve graded porosity or integration of dense and porous ceramic layers [27].

In recent studies on the development of SOFCs, infiltration of polymeric precursors of catalytically active materials into porous 8 mol% yttria stabilized zirconia (YSZ) electrodes has been a critical step for fuel cell fabrication [30–32]. Porous YSZ electrodes are required to provide sufficient porosity to allow infiltration of the precursors and transport of the reactant/product gases while affording structural integrity to maintain conductivity of oxygen ions. Hence, the desired YSZ electrode microstructure involves a dense matrix with a controlled pore structure.

Electrode tapes are laminated on either side of an electrolyte tape and co-sintered prior to the infiltration steps. Formation of pores in the electrode tapes and densification of the adjacent electrolyte layer introduces challenges impairing the integrity of their multilayer structure due to their dissimilar shrinkages. Various pore formers can be utilized to control the development of the porous electrodes. However, each pore former results in a different shrinkage profile on the tapes due to its characteristic particle morphology while it requires a controlled removal with a specific heating profile due to its particular thermal decomposition/oxidation behavior. As a result, undesired macroscopic defects such as cracks, blisters, warpage and delamination were observed as the compositions of the electrode tapes were modified to improve the performance of the SOFCs by changing the type, size and loading of the pyrolyzable pore formers. Therefore, a systematic study was needed to understand the relations between the properties of the pore formers, the resultant pore structures and the dimensional changes upon their removal and sintering. The gained knowledge would allow developing fabrication routes for defect-free (e.g. cracks, delaminations, blisters and warpage) multilayer ceramics.

Pore forming materials were selected considering their desired properties. Selection criteria included particle size and shape for a better understanding of the effect of the pore former morphology on the final pore structure, and decomposition/oxidation of pore formers with a minimum amount of residual carbon and other trace impurities that can affect the sintering behavior and properties of the YSZ matrix [33]. Selected high-purity pore formers had distinct morphological features such as plate-like flake graphite, spherical PMMA and polystyrene, spheroidal graphite and random shaped sucrose. Moreover, they demonstrated dissimilar particle size distributions ranging from monodisperse to bimodal and polydisperse.

Even though numerous studies were conducted using graphite [8,28,33,34], PMMA [26,28,35], sucrose [36,37] and polystyrene [38–40] as pore formers, the processing conditions such as fabrication techniques, matrix materials, compositions and sintering profiles were not comparable and it was relatively difficult to draw any useful conclusions about their pore forming features with respect to each other. Moreover, the effect of the pore formers on the evolution of the final pore structures and the dimensional changes of the ceramics were not reported in sufficient detail towards processing of crack-free porous ceramic tapes. Therefore, a detailed comparative investigation of the pore formers is aimed by this study to reveal the relationships between their particle characteristics, processing conditions and effect on the pore structures of ceramics as well as dimensional changes during sintering of porous tape-cast ceramics.

Various techniques were employed for detailed analyses of the properties of the pore former particles such as size, shape, distribution, surface area and decomposition/oxidation behavior. The compositions of the ceramic slurries were developed for tape casting and lamination using identical volume fractions of the components for all of the pore formers for a consistent comparison. The analysis of their effects on the rheological properties of ceramic slurries in identical conditions provided additional information on their particle characteristics while characterization of their thermal properties allowed determining heating profiles for their defect-free removal from tape-cast multilayer ceramics. Detailed investigations on the final microstructures led to a better understanding of the pore former – microstructure relationships of the sintered porous ceramics.

2. Experimental procedure

Commercially available high purity powders of flake and spheroidal graphite (Superior Graphite, Chicago, IL, USA), spherical polymethyl methacrylate (PMMA) (Sekisui, Osaka, Japan), random shaped sucrose (Alfa Aesar, Ward Hill, MA, USA) and spherical polystyrene (Alfa Aesar, Ward Hill, MA, USA) were selected. Although various starch types are also common pore formers, they were not included in this study due to the swelling phenomenon at elevated temperatures which makes it difficult to predict the final porosity by considering the initial properties and loading of the pore formers [41–43]. All pore formers were characterized as received except sucrose. Since it was not supplied with a certain particle specification, it was sifted through a 325 mesh screen.

Pore former particles were dispersed in an ethanol (Sigma-Aldrich, St. Louis, MO, USA) and toluene (Sigma-Aldrich, St. Louis, MO, USA) mixture and lightly

coated on aluminum stubs prior to analyzing their morphologies. The coated particles were investigated using a scanning electron microscope (FE-SEM, S-4700, Hitachi, Tokyo, Japan).

Particle size distribution analysis was carried out in a laser diffraction analyzer (S3500, Microtrac, Largo, FL, USA) by using the conventional procedure [44,45]. All pore former particles were dispersed in distilled water at the sample preparation stage except sucrose. Sucrose was dispersed in isopropyl alcohol (Sigma-Aldrich, St. Louis, MO, USA) to avoid its solubility in water. Each measurement was repeated three times and the average was taken for the results.

Surface area measurements of the pore former particles were conducted using a surface area analyzer (NOVA 2000e, Quantachrome, Boynton Beach, FL, USA). Measurements were repeated twice and compared for their accuracy. A standard procedure was employed for the analysis of the B.E.T. (Brunauer–Emmet–Teller) gas adsorption measurement results [46].

Thermogravimetric analysis (TGA) and differential thermal analysis (DTA) of the pore formers were performed in a TGA/DTA unit (STA 409C, Netzsch, Selb, Germany) simultaneously in order to analyze their decomposition/oxidation behavior. Heating rate of 10 °C/min was used up to 1200 °C for the measurements in air. The same thermal analyses were performed also for a conventional binder system, polyvinyl butyral (PVB-79, Monsanto, St. Louis, MO, USA) plasticized with dioctyl phthalate (DOP, Sigma-Aldrich, St. Louis, MO, USA), as a reference for developing heating profiles for laminated ceramic tapes.

Ceramic slurries were prepared using a three stage preparation technique. In the first stage, YSZ powder (TZ-8Y, Tosoh, Tokyo, Japan), solvents (ethanol and toluene) and dispersant (KD-1, ICI, Barcelona, Spain) were mixed for one day by ball milling to achieve a homogeneously dispersed suspension. A mixture of ethanol (40 wt%) and toluene (60 wt%) was used as solvent for slurry preparation. The dispersant, KD-1, is a polyester/polyamine copolymer with an estimated molecular weight of ~10,000 g/mol and has been efficiently used for dispersing a wide range of ceramic powders [47,48]. In the second stage, the binder (PVB-79) and the plasticizer (DOP) were added to the slurry and milled for one day. The third stage consisted of the addition of pore formers to the slurry and further milling for one more day to achieve homogeneous distribution of the constituents. Sucrose is slightly soluble in ethanol [49] while it is insoluble in toluene [50]. The azeotropic mixture of toluene and ethanol [51] used for the slurry preparation demonstrated negligible solubility of sucrose. Therefore, sucrose particles maintained their physical features in the prepared slurries. The mixed slurries were then degassed for 5 min under vacuum prior to viscosity measurements and tape casting.

Viscosity measurements were performed to investigate the effect of the pore formers on the rheological properties of the slurries. A viscometer (VT550, Haake, Karlsruhe, Germany) was utilized for the measurements by applying shear rates ranging from 0 s^{-1} to 100 s^{-1}.

The measured thickness of the dry tapes was between 100 and 120 μm. Tapes were laminated at 80 °C using a pressure of 25 MPa to obtain an average thickness of 625 μm (± 25 μm) after lamination. The laminates were then heated in air to remove the organic content as well as the pore formers. Binder removal was conducted using a controlled heating profile to avoid macroscopic defects such as cracks, delamination and blistering. TGA analysis of the components (pore formers and binder/plasticizer) was utilized to optimize heating profiles for their defect-free burnout [27]. All samples were sintered in air at 1350 °C for 2 h after the burnout of the pyrolyzable components (binder, plasticizer, dispersant and pore former particles).

Dimension and weight changes of the samples were measured before and after burnout and sintering steps to analyze the effect of burnout and sintering processes on the laminated tapes. Final microstructures of the porous YSZ samples were investigated using SEM on the fractured cross-sections. Porosity, pore size distribution and pore connectivity of the samples were characterized using a mercury intrusion porosimeter (PoreMaster 60, Quantachrome, Boynton Beach, FL, USA). The measurements were performed in a wide range of applied pressures (101.33 kPa–68.95 MPa) for a detailed analysis of pore structures [26,52].

3. Results and discussion

3.1. Particle characteristics of the pore formers

Flake graphite and sucrose showed the most anisometric and highly polydisperse particles while spheroidal graphite consisted of more monodisperse particles with higher isometric features as shown in the micrographs presented in Fig. 1. Although most synthetic polymers are polydisperse [38], polystyrene showed highly monodisperse particles with relatively high spherical isometry. PMMA revealed a relatively large amount of small particles beside the large particles indicating a bimodal distribution of particles as shown in Fig. 2(c).

Quantification of the observations made on the micrographs is necessary for a better understanding of the characteristics of the pore formers. Therefore, laser diffraction measurements were performed on the pore former particles. As seen in Fig. 2., flake graphite (a) and sucrose (d) showed relatively broad number weighted particle size distributions (frequency histograms) that are in agreement with the obtained micrographs in Fig. 1. Broad size distributions of flake graphite and sucrose particles involve deviation from ideal polydispersion as characterized by the distinguishable difference between their characteristic statistic parameters such as mode, median and average particle size as summarized in Table 1. The abundance of

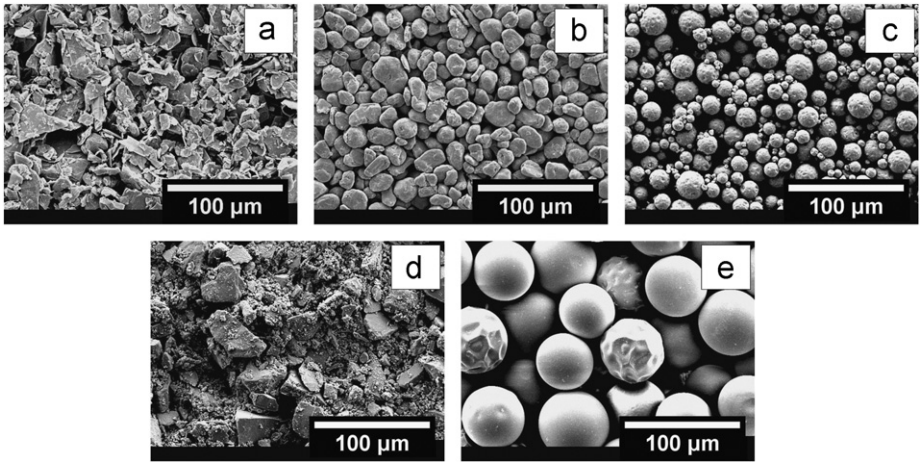

Fig. 1. Scanning electron micrographs of (a) flake graphite, (b) spheroidal graphite, (c) PMMA, (d) sucrose and (e) polystyrene particles.

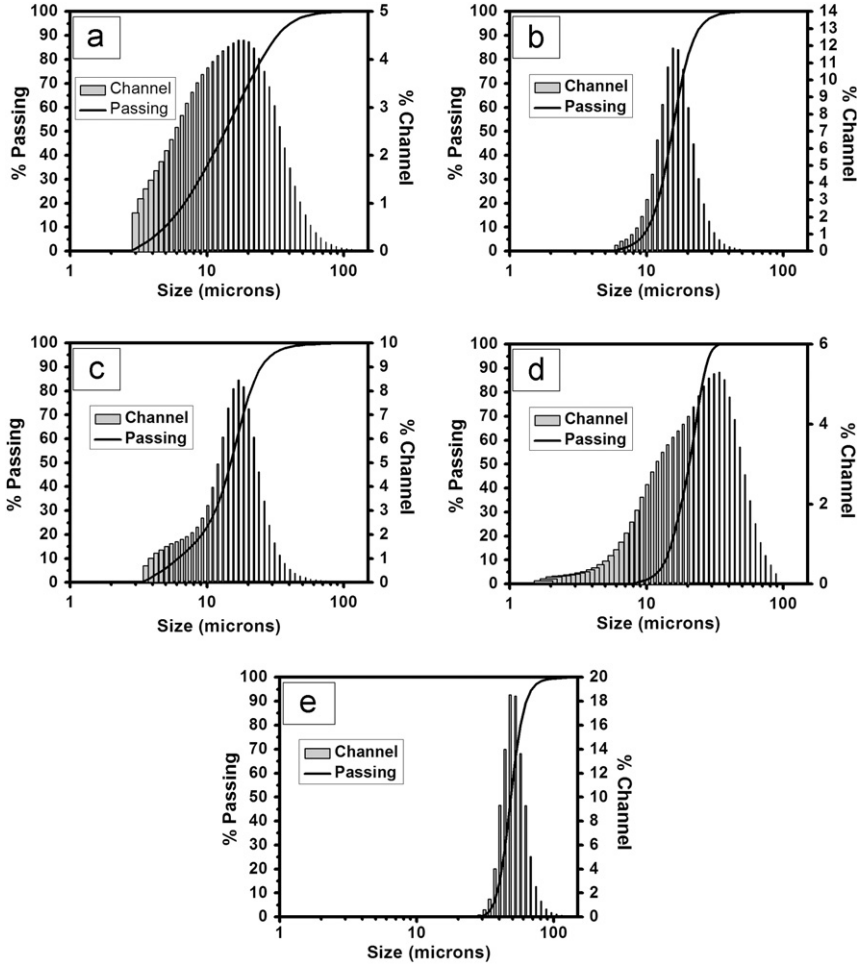

Fig. 2. Number weighted particle size distributions of (a) flake graphite, (b) spheroidal graphite, (c) PMMA, (d) sucrose and (e) polystyrene particles.

the smaller particles dominated the size distributions and resulted in smaller medians and average particle sizes. Since spheroidal graphite and polystyrene demonstrated relatively narrow particle size distributions, the analysis of these particles did not reveal any significant difference between the mode, the median and the average particle size. PMMA particles also showed a similar narrow distribution; however, their tendency toward bimodal distribution resulted in considerable difference between the characteristic statistic parameters of their distribution.

Although mode and median of the distribution were close to each other, higher number of small particles led to a relatively small average particle size.

Although flake graphite was expected to have higher surface area considering its relatively smaller and anisometric particles, the surface roughness of the spheroidal graphite yielded considerably high surface area as shown in Table 1. While the measured surface areas of the hydrocarbon based pore formers were substantially lower due to limited surface roughness, size and distribution of their particles determined their surface areas. Therefore, the lowest surface area was measured on polystyrene pore formers due to relatively large size and highly monodisperse particles. Although both pore formers were nearly isometric, PMMA particles demonstrated an order of magnitude higher surface area than polystyrene due to polydisperse and smaller size of particles.

3.2. Effect of the pore formers on the rheological properties of the ceramic slurries

Incorporation of pore formers results in distinguishable changes in the rheological properties of the slurries. Loading of the pore former particles in the slurries as well as their particle characteristics such as size, shape and distribution gives rise to particle to particle interactions which in turn lead to an increase in the viscosity. Thus, the recipe of slurries needs to be optimized by controlling the binder and dispersant ratios to obtain a suitable viscosity for casting of defect-free tapes. However, changing the binder loading may also alter the shrinkage of the sintered porous ceramics [27]. Since the binder itself acts as a pore former, any increase in the amount of the binder would introduce additional porosity to the tapes after the burnout process [28] and the comparison would be biased. Therefore, the slurry compositions were optimized by using the same volumetric loading of ceramic powder, dispersant, binder and pore former in ceramic tapes for a consistent comparison as shown in Table 2.

Table 1
Particle size and surface area characteristics of the pore formers.

	Flake graphite	Spheroidal graphite	PMMA	Sucrose	Polystyrene
Mode (μm)	18.05	15.56	16.96	33.93	47.98
Median particle size (d_{50}) (μm)	13.57	15.42	14.93	22.64	48.40
Average particle size (μm)	6.59	13.09	8.39	4.14	46.37
Surface area (m^2/g)	4.526	5.45	1.168	0.771	0.106

The optimization of the slurry compositions involved their resultant rheological properties such as viscosity and shear thinning behavior to perform a successful tape casting using the same amount of solvents. The optimized ratio of the solvent to the ceramic powder was determined at ~90 wt% and kept constant for all of the slurries. As a result, slurry viscosities were maintained in a reasonable range (4–20 Pa s) for tape casting [53,54]. A desired shear-thinning behavior of the slurries was observed with the increase of the shear rate as shown in Fig. 3.

Although addition of the pore formers to the slurries resulted in similar rheological properties, their particle characteristics gave rise to distinguishable differences in the resultant viscosities. Since relatively anisometric particles of flake graphite led to increased particle to particle interactions, their incorporation resulted in a higher viscosity than the relatively isometric particles of spheroidal graphite. Even though both PMMA and polystyrene particles were relatively isometric, monodisperse polystyrene particles with relatively strong particle to particle interactions gave rise to the resultant viscosity of the slurry. Their significantly broad distribution especially in

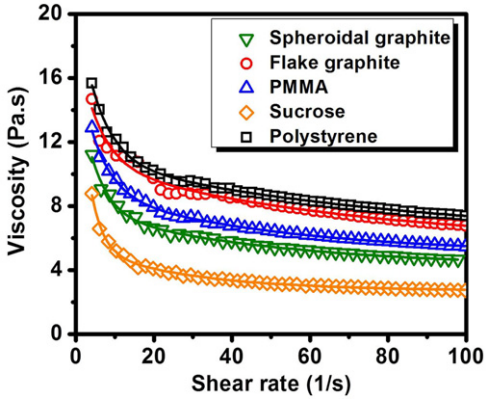

Fig. 3. Viscosities of the tape casting slurries with various pore formers as a function of applied shear rate.

Table 2
Compositions of the green tapes in weight and volume percents for various pore formers.

Pore former	YSZ		Dispersant		Binder		Plasticizer		Pore former	
Type	**wt%**	**vol%**	**wt%**	**vol%**	**wt%**	**vol%**	**wt%**	**vol%**	**wt%**	**vol%**
Flake graphite	61.7	28.6	0.3	0.7	11.5	29.5	5.8	15.9	20.7	25.3
Spheroidal graphite	61.7	28.6	0.3	0.7	11.5	29.5	5.8	15.9	20.7	25.3
PMMA	72.8	28.6	0.3	0.7	13.6	29.5	6.8	15.9	6.5	25.3
Sucrose	65.8	28.6	0.3	0.7	12.3	29.5	6.2	15.9	15.4	25.3
Polystyrene	69.4	28.6	0.3	0.7	13	29.5	6.5	15.9	10.8	25.3

relatively small sizes limited the interactions of the sucrose particles. Therefore, incorporation of the sucrose particles to the slurry composition resulted in the lowest increase in the viscosity.

3.3. Thermal analysis of the pore formers

Thermal decomposition/oxidation behavior of the pore formers during the ceramic processes is determined by (i) the surrounding atmosphere, (ii) the heating rate and (iii) the temperature. Fig. 4 shows thermogravimetric curves of flake graphite, spheroidal graphite, PMMA, sucrose and polystyrene as well as PVB samples measured with a heating rate of 10 °C/min in air. Although both polymer based pore formers, PMMA and polystyrene, started losing mass around 165 °C and 250 °C, their fastest mass losses were observed around 265 °C and 350 °C, respectively. PVB started losing weight around 213 °C and its maximum decomposition and mass loss was observed around 350 °C. All hydrocarbon based samples showed complete decomposition below 600 °C as shown in Fig. 4(a).

Weight loss was not observed with either graphite sample up to 600 °C as shown in Fig. 4(b). The initial mass losses of flake graphite and spheroidal graphite were observed around 619 °C and 600 °C, respectively. This is in a good agreement with the investigations reported in the literature [55,56]. Oxidation of the crystalline graphite took place at a relatively slow rate with respect to the decomposition of amorphous polymers (e.g. PMMA and polystyrene) and crystalline sucrose as summarized in Table 3. Although spheroidal graphite is expected to show faster oxidation kinetics than flake graphite considering its higher surface area (Table 1), oxidation of the flake graphite was significantly faster. The initial surface roughness of the spheroidal graphite gave rise to its initial oxidation kinetics at lower temperatures; however, the high aspect ratio and smaller size of flake graphite particles allowed their oxidation to reach higher rates and to complete at lower temperatures.

Although all hydrocarbon based pore formers and the binder decomposed considerably faster than the oxidation of the crystalline graphites, sucrose decomposed significantly slower than the PMMA, polystyrene and binder. Sucrose melted before it started losing mass as it was characterized using simultaneous TGA-DTA measurements. An endothermic effect was observed at around 160 °C corresponding to a melting process which was also confirmed by investigations performed on a temperature controlled hot plate. The slower decomposition kinetics of sucrose was attributed to the loss of its surface area as it was transformed to the liquid phase.

3.4. Sintering characteristics and analysis of the microstructures

Thermogravimetric analysis of the pore formers and plasticized binder allowed controlling of the burnout stages to eliminate rapid outlet of decomposition/oxidation

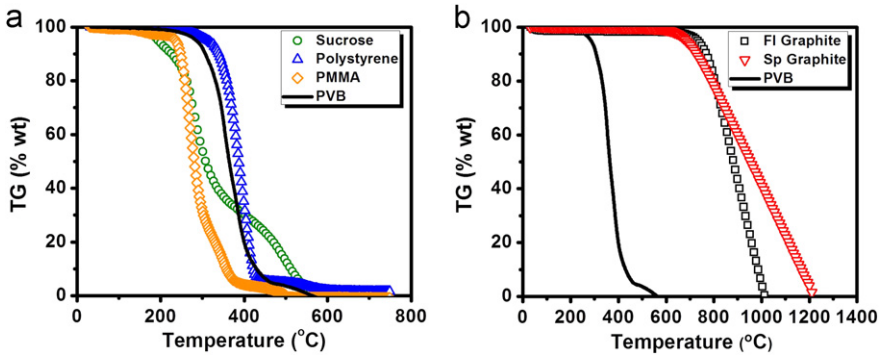

Fig. 4. Thermogravimetric analysis of (a) the hydrocarbon based pore formers and (b) the graphite based pore formers with respect to the plasticized binder (PVB).

Table 3
Decomposition/oxidation parameters of the pore formers and the plasticized binder (PVB).

Pore former Type	Initial decomposition temperature (°C)	Onset decomposition temperature (°C)	Maximum decomposition temperature (°C)	Maximum decomposition rate (g/min)	Final decomposition temperature (°C)
Flake graphite	618.93	758.34	863.79	3.982	1013.91
Spheroidal graphite	599.68	690.77	1015.13	1.86	1198.68
PMMA	164.31	253.73	263.28	13.6	500.45
Sucrose	175.54	234.21	273.02	7.613	591.5
Polystyrene	249.33	352.82	385.71	13.1	598.32
PVB	212.51	316.48	349.5	10.81	589.54

gases and defect formation in the laminated tapes. Heating rate of 5.0 °C/min was applied up to the sintering temperature of 1350 °C after the soaking steps were applied at the identified controlled removal temperatures of the pore formers and the binder. The identified controlled decomposition temperatures for polystyrene, PMMA and sucrose pore formers were 310 °C, 210 °C and 180 °C, respectively. Their samples were first heated up to the decomposition temperature of pore formers with the heating rate of 0.5 °C/min and held for one hour to complete the burnout followed by heating to the decomposition temperature of the binder at 320 °C. Since the controlled oxidation temperature of flake graphite and spheroidal graphite was identified as 600 °C, decomposition of the binder took place before their oxidation. Considering the sluggish oxidation of graphite, samples were kept at 600 °C for two hours. The samples were then heated to the sintering temperature of 1350 °C with the heating rate of 5.0 °C/min and held for two hours followed by cooling to the room temperature at a rate of 5.0 °C/min.

Macroscopic defects, such as warpage, delamination, and cracks were not observed in the samples after sintering. This was the evidence that casting and drying did not result in inhomogeneous tape compositions. Dimensional changes and the weight losses of the laminated tapes after removal of the pore formers and binder are summarized in Table 4. The solvents used for the slurry preparation were expected to leave the tapes upon drying prior to lamination. It was confirmed by measuring the weight of the laminated tapes before and after burnout. Measured weight losses of all five tape compositions were in a good agreement with the dry tape compositions shown in Table 2.

Although YSZ particles could not be sintered by firing at 800 °C for one hour after the removal of the binder and the pore formers, dimensional changes were observed in the laminates (Table 4). It is known that excess binder allows further densification and increases shrinkage in tape-cast ceramics since it forms fine closed porosity by improving the packing density of ceramic particles due to its migration before decomposition [8,28,33]. Therefore, the observed partial densification of the laminated tapes after removal of their pyrolyzable content was attributed to an increase of the packing density of YSZ particles by migration of the binder. Since incorporated graphite particles were removed from the tapes at relatively high temperatures (Table 3), they did not leave pores available for migration of the binder before its decomposition. Thus, the effect of the binder migration was lower for graphite containing tapes. However, hydrocarbon based pore formers decomposes earlier than the binder. It allowed the binder to migrate into the pores and increase the packing density of the YSZ particles further as summarized in Table 4. Sucrose incorporated tapes exhibited relatively high shrinkage upon removal of the pore former particles and the binder. The additional increase in the packing of the YSZ particles was attributed to the migration of the molten sucrose similar to the binder prior to its decomposition.

Table 4
Dimensional changes and weight losses of the laminated dry tapes after removal of pyrolyzable components and firing at 800 °C for one hour.

Tape	Volume change (%)	Diameter change (%)	Thickness change (%)	Weight loss (%)
Flake graphite	−4.19	−2.14	−0.05	39.21
Spheroidal graphite	−6.65	−2.70	−1.40	39.19
PMMA	−9.32	−3.7	−2.24	28
Sucrose	−17.49	−6.29	−6.05	35.24
Polystyrene	−9.54	−5.67	−1.65	31.60

It is evident that the morphological features of the pore formers are replicated in the final porous microstructures as shown in Fig. 5. Isometric features of spheroidal graphite, PMMA and polystyrene particles resulted in nearly spherical pores. Flake graphite yielded anisometric pores representing its plate like geometry with the preferential orientation along the tape casting direction as sucrose also maintained its anisometry in the sintered microstructure but lost its broad particle size distribution due to melting of sucrose particles. Hence, the expected large pores left by the initial large particles of sucrose (Fig. 1(d)) were not observed in the sintered ceramics as shown in Fig. 5(d).

The volume change after sintering was around 56% for all samples except the sucrose sample as summarized in Table 5. The aforementioned thermal behavior of sucrose resulted in an additional densification of the porous matrix due to improved packing of the YSZ particles.

Further characterization of the sintered microstructures was performed using mercury intrusion porosimetry technique. Although the intruded pore sizes between 2 μm and 200 μm were in a good agreement with the pore sizes observed in the micrographs shown in Fig. 5, significant amount of intrusion took place in a range of small pore sizes below 2 μm for all samples except the sample prepared by removal of PMMA particles. Since it was previously observed in the investigations on the tape-cast YSZ electrolyte layers that near complete density can be achieved using identical sintering temperature (1350 °C) and time (2 h), the formed porosity is attributed to the removal of the incorporated pore former particles. However, this range of the pore sizes was relatively smaller than the initial particle sizes of the pore formers shown in Fig. 6. It suggests that the pores were connected through smaller channels which allow the intrusion of mercury at elevated pressures.

Interconnected porosity can be achieved by percolation of the pore former particles [8,28,29]. High aspect ratio ($\gg 1$) of the particles of the flake graphite led to a percolating network by bridging of the pore former particles at the same volumetric loading [22]. Thus flake graphite allowed achieving almost completely open pores

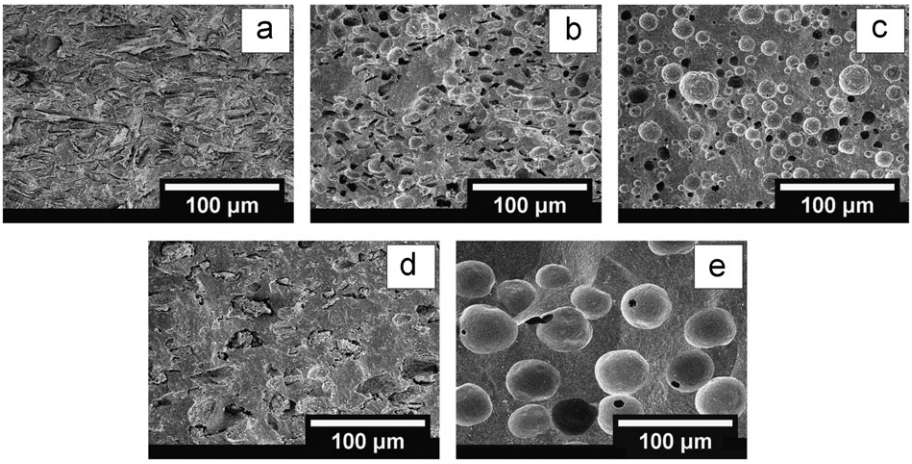

Fig. 5. Scanning electron micrographs of the cross sections of the sintered porous YSZ samples prepared by removal of (a) flake graphite, (b) spheroidal graphite, (c) PMMA, (d) sucrose and (e) polystyrene pore formers.

Table 5
Dimensional changes and weight losses of the laminated dry tapes after sintering.

Tape	Volume change (%)	Diameter change (%)	Thickness change (%)	Weight loss (%)
Flake graphite	−56.59	−24.46	−23.93	39.11
Spheroidal graphite	−56.72	−24.89	−23.29	39.21
PMMA	−55.87	−25.43	−25.64	28
Sucrose	−64.14	−29.21	−28.43	35.43
Polystyrene	−57.51	−27.14	−19.93	31.21

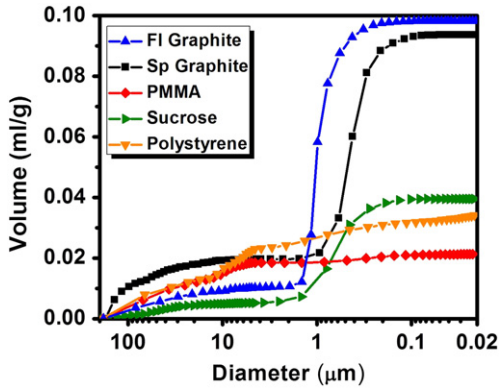

Fig. 6. Pore size distribution of the sintered tapes characterized by the mercury intrusion porosimetry.

at around 35% bulk porosity. It demonstrated the highest amount of the intrusion of Hg and the lowest amount of closed porosity (~0.65%) among the fabricated porous ceramics in this study. Almost entirely open porosity achieved by one of the commonly used pyrolyzable pore formers, flake graphite, can be considered as a reference for the comparison of pore forming characteristics of the other pore former particles at the same volumetric loading.

Spheroidal graphite samples showed the highest amount of the large pores (2–200 µm) while sucrose samples showed the lowest amount of the large pores due to melting of its particles prior to decomposition. Higher densification of the sucrose also resulted in the lowest bulk porosity of 27.01%, as shown in Table 6. Spheroidal graphite yielded less open porosity (27.59%) than flake graphite due to its relatively isometric particles. Although PMMA yielded 27.08% bulk porosity, only 10% of the porosity was open due to disconnected PMMA particles in the initial tape. Since pores left by PMMA did not percolate, intrusion did not take place in the pore sizes below 2 µm. Polystyrene particles achieved the percolation at the same volumetric loading due to their uniform size and resulted in more open porosity than PMMA although both are relatively isometric. Bimodal size distribution of PMMA particles resulted in disconnection of the final pores and the highest amount of measured closed porosity (24.38%). Moreover, although PMMA has a similar particle size distribution to the spheroidal graphite, its decomposition at lower temperatures prior to the decomposition of the binder, PVB, led to closing of the smaller pores. As the density of the matrix increased at the expense of closing small pores, the porosity left by larger PMMA particles got isolated and it gave rise to the closed porosity. The monodisperse particles of polystyrene left uniform pores surrounded with a dense matrix which resulted in 22.29% closed porosity.

Table 6
Measured bulk, open and closed porosities of the sintered tapes.

	Flake graphite	Spheroidal graphite	PMMA	Sucrose	Polystyrene
Bulk porosity (%)	35.92	35.72	27.08	22.01	32.9
Open porosity (%)	35.27	27.59	2.69	17.55	10.61
Closed porosity (%)	0.65	8.13	24.38	4.46	22.29

Although the binder left the laminated structure earlier than both flake and spheroidal graphites, it did not result

in any cracks due to structural weakening during their oxidation. Moreover, earlier removal of the binder at around 320 °C eliminated further improvement of the packing of the ceramic particles in the graphite containing tapes by binder migration through the formed porosity. However, hydrocarbon based pore formers decomposing at temperatures lower than the decomposition temperature of the binder could not eliminate this phenomenon and yielded lower bulk porosities than the graphite based pore formers. Sucrose demonstrated the lowest amount of bulk porosity with its decomposition at the lowest measured decomposition temperature (~180 °C) while polystyrene showed higher bulk porosity than both sucrose and PMMA with its decomposition at a temperature (~310 °C) close to the decomposition temperature of the binder. Furthermore, both flake and spheroidal graphite yielded almost the same amount of bulk porosity (~36%) even though their particles have distinct morphological properties. As discussed earlier, the shape of the particles induced their percolation and identified the amount of open porosity; however, the amount of the bulk porosity was not significantly affected by the morphological features of the graphite based pore formers. Thus, the sequence of the removal of binder and pore formers can explain the higher bulk porosities achieved by utilizing graphite particles as pore formers (Table 6).

4. Summary and conclusions

Morphological and dimensional characteristics of pore formers were investigated using SEM micrographs and B.E.T. surface area measurements while distributions of the particle sizes were quantified using laser diffraction technique. Sucrose and flake graphite showed relatively broad size distributions with random shaped particles while spheroidal graphite, PMMA and polystyrene showed more spherical particles with narrow size distributions. Polydisperse particles of flake graphite and sucrose might be considered for porous structures where decreased tortuosity is required with open porosity; however, melting of sucrose prior to decomposition may eliminate its pore forming capabilities.

Polymer based pore formers, PMMA and polystyrene, demonstrated the largest portion of the mass loss between 250 °C and 400 °C which was comparable to the burnout profile of the evaluated conventional binder, PVB. Completing the burnout step for all of the pyrolyzable content in such a narrow temperature range allowed completing the heating profile of the porous ceramics in a short period of time. Since the controlled burnout can be completed at temperatures as low as 350 °C, it may allow processing of the compositions sensitive to high temperature oxidation.

Oxidation of both flake and spheroidal graphite pore formers took place relatively slowly with respect to the hydrocarbon based pore formers. Although spheroidal graphite had a larger initial surface area, flake graphite oxidized faster than the spheroidal graphite due to its plate-like shape and smaller particles allowing higher surface area as the oxidation proceeds. Therefore, size and shape as well as surface area of the graphite particles need to be taken into account while planning heating profiles for processing of porous ceramics. Incorporation of graphite to ceramic tapes as pore former may not require a slow heating profile for a defect-free burnout step.

Investigated pore formers acted as templates for the yielded porosities by means of pore shape, size and connectivity. Sucrose was the only exception since it lost the initial characteristics of its particles upon melting. All pore formers analyzed in this study resulted in similar amounts of volume change after sintering except sucrose. As highly isometric particles of PMMA yielded highest amount of closed porosity, anisometric particles of the flake graphite yielded highest amount of open porosity at the same volumetric loading. The achieved bulk porosity was strongly affected by the removal sequence of the pore formers. While sucrose yielded the lowest bulk porosity with its decomposition at lower temperatures, graphite based pore formers oxidizing at elevated temperatures formed the highest amount of bulk porosity. Although the morphology of the pore former particles had a significant influence on the amount of the formed open porosity, the amount of the bulk porosity was not affected by the shape of the graphite particles.

It is demonstrated that the thermal and morphological properties of the pore formers have a vital effect on the features of resultant microstructures. Desired tape-cast porous ceramics can be fabricated without defects by using various pore formers, provided that the processing parameters are identified and adjusted accordingly. Therefore, the obtained understanding of the relationships between pore formers and resulted pore structures as well as the identified processing parameters will be utilized for the improvement of multilayer structures and the development of planar SOFCs.

Acknowledgments

This work was supported by a grant of the AFRL under contract no. FA4819-09-C-0018. Utilization of SEM facilities at the Graduate Center for Materials Research (MRC) of Missouri University of Science and Technology is greatly acknowledged.

References

[1] T. Tsuru, Inorganic porous membranes for liquid phase separation, Separation & Purification Reviews 30 (2001) 191–220.
[2] J. She, T. Ohji, Z.-Y. Deng, Thermal shock behavior of porous silicon carbide ceramics, Journal of the American Ceramic Society 85 (2002) 2125–2127.
[3] M.L. Dunn, M. Taya, Electromechanical properties of porous piezoelectric ceramics, Journal of the American Ceramic Society 76 (1993) 1697–1706.

[4] C.P. Shaw, R.W. Whatmore, J.R. Alcock, Porous, functionally gradient pyroelectric materials, Journal of the American Ceramic Society 90 (2007) 137–142.
[5] L. Yin, H.X. Peng, L. Yang, B. Su, Fabrication of three-dimensional inter-connective porous ceramics via ceramic green machining and bonding, Journal of the European Ceramic Society 28 (2008) 531–537.
[6] A.R. Walpole, Z. Xia, C.W. Wilson, J.T. Triffitt, P.R. Wilshaw, A novel nano-porous alumina biomaterial with potential for loading with bioactive materials, Journal of Biomedical Materials Research Part A 90 (2009) 46–54.
[7] X. Huang, Separator technologies for lithium-ion batteries, Journal of Solid State Electrochemistry 15 (2011) 649–672.
[8] S.F. Cobin, P.S. Apté, Engineered porosity via tape casting, lamination and the percolation of pyrolyzable particulates, Journal of the American Ceramic Society 82 (1999) 1693–1701.
[9] G.T. Chandrappa, N. Steunou, J. Livage, Macroporous crystalline vanadium oxide foam, Nature 416 (2002) 702.
[10] Z. Zivcová, E. Gregorová, W. Pabst, Low- and high-temperature processes and mechanisms in the preparation of porous ceramics via starch consolidation casting, Starch/Stärke 62 (2010) 3–10.
[11] J.R. Wilson, S.A. Barnett, Solid oxide fuel cell Ni-YSZ anodes: effect of composition on microstructure and performance, Electrochemical and Solid-State Letters 11 (2008) B181–B185.
[12] D. Simwonis, F. Tietz, D. Stöver, Nickel coarsening in annealed Ni/8YSZ anode substrates for solid oxide fuel cells, Solid State Ionics 132 (2000) 241–251.
[13] A. Sarikaya, V. Petrovsky, F. Dogan, Effect of the anode microstructure on the enhanced performance of solid oxide fuel cells, International Journal of Hydrogen Energy, doi: 10.1016/j.ijhydene.2012.05.007, in press.
[14] D. Chen, B. Zhang, H. Zhuang, W. Li, Combustion synthesis of network silicon nitride porous ceramics, Ceramics International 28 (2003) 363–364.
[15] K. Maca, P. Dobsak, A.R. Boccaccini, Fabrication of graded porous ceramics using alumina–carbon powder mixtures, Ceramics International 27 (2001) 577–584.
[16] X. Mao, S. Wang, S. Shimai, Porous ceramics with tri-modal pores prepared by foaming and starch consolidation, Ceramics International 34 (2008) 107–112.
[17] J.-M. Qian, Z.-H. Jin, X.W. Wang, Porous SiC ceramics fabricated by reactive infiltration of gaseous silicon into charcoal, Ceramics International 30 (2004) 947–951.
[18] T. Fukasawa, M. Ando, T. Ohji, S. Kanzaki, Synthesis of porous ceramics with complex pore structure by freeze-dry processing, Journal of the American Ceramic Society 84 (2001) 230–232.
[19] Y.-W. Kim, S.-H. Kim, C. Wang, C.B. Park, Fabrication of microcellular ceramics using gaseous carbon dioxide, Journal of the American Ceramic Society 86 (2003) 2231–2233.
[20] A. Nakahira, F. Nishimura, S. Kato, M. Iwata, S. Takeda, Green fabrication of porous ceramics using an aqueous electrophoretic deposition process, Journal of the American Ceramic Society 86 (2003) 1230–1232.
[21] Y. Gu, X. Liu, G. Meng, D. Peng, Porous YSZ ceramics by water-based gelcasting, Ceramics International 25 (1999) 705–709.
[22] A. Mortensen, S. Suresh, Functionally graded metals and metal–ceramic composites: part 1—processing, International Materials Reviews 40 (1995) 239–265.
[23] J.F. Yang, G.J. Zhang, T. Ohji, Porosity and microstructure control of porous ceramics by partial hot pressing, Journal of Materials Research 16 (2001) 1916–1918.
[24] S. Zhu, S. Ding, H. Xi, Q. Li, R. Wang, Preparation and characterization of SiC/cordierite composite porous ceramics, Ceramics International 33 (2007) 115–118.
[25] L. Hu, C.-A. Wang, Y. Huang, Porous yttria-stabilized zirconia ceramics with ultra-low thermal conductivity, Journal of Materials Science 45 (2010) 3242–3246.
[26] H.L. Zhang, J.-F. Li, B.-P. Zhang, Microstructure and electrical properties of porous PZT ceramics derived from different pore-forming agents, Acta Materialia 55 (2007) 171–181.
[27] S.F. Corbin, J. Lee, X. Qiao, Influence of green formulation and pyrolyzable particulates on the porous microstructure and sintering characteristics of tape cast ceramics, Journal of the American Ceramic Society 84 (2001) 41–47.
[28] M. Boaro, J.M. Vohs, R.J. Goerte, Synthesis of highly porous yttria-stabilized zirconia by tape-casting methods, Journal of the American Ceramic Society 86 (2003) 395–400.
[29] J.-H. Lee, J.-W. Heo, D.-S. Lee, J. Kim, G.-H. Kim, H.-W. Lee, H.S. Song, H.-H. Moon, The impact of anode microstructure on the power generating characteristics of SOFC, Solid State Ionics 158 (2003) 225–232.
[30] A. Buyukaksoy, V. Petrovsky, F. Dogan, Stability and performance of solid oxide fuel cells with nanocomposite electrodes, Journal of the Electrochemical Society 159 (2012) B666–B669.
[31] J.M. Vohs, R.J. Gorte, High-performance SOFC cathodes prepared by infiltration, Advanced Materials 21 (2009) 943–956.
[32] T.J. Armstrong, J.G. Rich, Anode-supported solid oxide fuel cells with $La_{0.6}Sr_{0.4}CoO_3$–$Zr_{0.84}Y_{0.16}O_2$ composite cathodes fabricated by an infiltration method, Journal of the Electrochemical Society 153 (2006) A515–A520.
[33] A. Sanson, P. Pinasco, E. Roncari, Influence of pore formers on slurry composition and microstructure of tape cast supporting anodes for SOFCs, Journal of the European Ceramic Society 28 (2008) 1221–1226.
[34] J.H. Choi, T. Lee, T.-S. Park, K.-B. Yoo, Y.-S. Yoo, Microstructure and performance of anode supported cell by pore size of anode, in: J. Weidner, S.R. Narayanan (Eds.), Battery and Energy Technology (General)—214th ECS Meeting/PRIME 2008, ECS Transactions, vol. 16, The Electrochemical Society, Pennington, NJ, 2009, pp. 37–42.
[35] F. Tang, H. Fudouzi, T. Uchikoshi, Y. Sakka, Preparation of porous materials with controlled pore size and porosity, Journal of the European Ceramic Society 24 (2004) 341–344.
[36] C. Wang, T. Kasuga, M. Nogami, Macroporous calcium phosphate glass-ceramic prepared by two-step pressing technique and using sucrose as a pore former, Journal of Materials Science: Materials in Medicine 16 (2005) 739–744.
[37] A.-M. Le Raya, H. Gautier, J.-M. Bouler, P. Weiss, C. Merle, A new technological procedure using sucrose as porogen compound to manufacture porous biphasic calcium phosphate ceramics of appropriate micro- and macrostructure, Ceramics International 36 (2010) 93–101.
[38] Y. de Hazan, V. Märkl, J. Heinecke, C. Aneziris, T. Graule, Functional ceramic and nanocomposite fibers, cellular articles and microspheres via radiation curable colloidal dispersions, Journal of the European Ceramic Society 31 (2011) 2601–2611.
[39] H. Chen, K. Cheng, Z. Wang, W. Weng, G. Shen, P. Du, G. Han, Preparation of porous NiO–$Ce_{0.8}Sm_{0.2}O_{1.9}$ ceramics, Journal of Materials Science and Technology 26 (2010) 523–528.
[40] T. Kim, G. Liu, M. Boaro, S.-I. Lee, J.M. Vohs, R.J. Gorte, O.H. Al-Madhi, B.O. Dabbousi, A study of carbon formation and prevention in hydrocarbon-fueled SOFC, Journal of Power Sources. 155 (2006) 231–238.
[41] E. Gregorová, W. Pabst, Porosity and pore size control in starch consolidation casting of oxide ceramics—achievements and problems, Journal of the European Ceramic Society 27 (2007) 669–672.
[42] E. Gregorová, W. Pabst, I. Bohačenko, Characterization of different starch types for their application in ceramic processing, Journal of the European Ceramic Society 26 (2006) 1301–1309.
[43] R. Barea, M.I. Osendi, P. Miranzo, J.M.F. Ferreira, Fabrication of highly porous mullite materials, Journal of the American Ceramic Society 88 (2005) 777–779.
[44] T. Allen, 5th edition, Particle Size Measurement, vols. 1–2, Chapman & Hall, London, UK, 1997.
[45] R. Xu, Particle Size Characterization: Light Scattering Methods, Kluwer Academic Publishers, Dordrecht, Netherlands, 2000.
[46] J.U. Keller, R. Staudt, Gas Adsorption Equilibria: Experimental Methods and Adsorption Isotherms, Springer, Berlin, Germany, 2005.

[47] X. Xu, R. Fu, J.M.F. Ferreira, Effect of homogenizing procedures on the slip casting of reaction sialon suspensions, Ceramics International 30 (2004) 745–749.
[48] X. Xu, S. Mei, J.M.F. Ferreira, Fabrication of Si_3N_4–SiC nanocomposite ceramics through temperature-induced gelation and liquid phase sintering, Journal of the European Ceramic Society 3 (2006) 337–341.
[49] P. Beringer, Remington: the Science and Practice of Pharmacy, 21st ed., Lippincott Williams & Wilkins, Philadelphia, PA, USA, 2006.
[50] M. Asadi, Beet-sugar Handbook, John Wiley & Sons, Inc., Hoboken, NJ, USA, 2007.
[51] N. Suppakarn, H. Ishida, J.D. Cawley, Roles of poly (propylene glycol) during solvent-based lamination of ceramic green tapes, Journal of the American Ceramic Society 84 (2001) 289–294.
[52] X. Wei, A. Atkinson, Ceramic–metal interpenetrating network composites formed by electrodeposition, Journal of the Electrochemical Society 152 (2005) C513–C519.
[53] R.E. Mistler, E.R. Twiname, Tape Casting: Theory and Practice, The American Ceramic Society, Westerville, OH, USA, 2000.
[54] N. Straue, M. Rauscher, M. Dressler, A. Roosen, Tape casting of ITO green tapes for flexible electroluminescent lamp, Journal of the American Ceramic Society 95 (2012) 684–689.
[55] S. Ding, S. Zhu, Y. Zeng, D. Jiang, Effect of Y_2O_3 addition on the properties of reaction-bonded porous SiC ceramics, Ceramics International 32 (2006) 461–466.
[56] H. Birol, T. Maeder, P. Ryser, Application of graphite-based sacrificial layers for fabrication of LTCC (low temperature co-fired ceramic) membranes and micro-channels, Journal of Micromechanics and Microengineering 17 (2007) 50–60.